# Observation of enhanced infrared absorption in silicon supersaturated with gold by pulsed laser melting of nanometer-thick gold films

Philippe K. Chow, Wenjie Yang, Quentin Hudspeth, Shao Qi Lim, Jim S. Williams, and Jeffrey M. Warrender

Citation: Journal of Applied Physics **123**, 133101 (2018); doi: 10.1063/1.5015984
View online: https://doi.org/10.1063/1.5015984
View Table of Contents: http://aip.scitation.org/toc/jap/123/13
Published by the American Institute of Physics

**Articles you may be interested in**

Dual origin of room temperature sub-terahertz photoresponse in graphene field effect transistors
Applied Physics Letters **112**, 141101 (2018); 10.1063/1.5018151

Effect of layer number and metal-chloride dopant on multiple layers of graphene/porous Si solar cells
Journal of Applied Physics **123**, 123101 (2018); 10.1063/1.5013169

Graphene-induced modulation effects on magnetic plasmon in multilayer metal-dielectric-metal metamaterial
Applied Physics Letters **112**, 131101 (2018); 10.1063/1.5022870

Investigation of in-situ co-doping by Sb and P of germanium films grown on Si(001) by molecular beam epitaxy
Journal of Applied Physics **123**, 133102 (2018); 10.1063/1.5009327

Carrier-selective interlayer materials for silicon solar cell contacts
Journal of Applied Physics **123**, 143101 (2018); 10.1063/1.5020056

Terahertz radiation generation through the nonlinear interaction of Hermite and Laguerre Gaussian laser beams with collisional plasma: Field profile optimization
Journal of Applied Physics **123**, 153101 (2018); 10.1063/1.5019430

AIP | Journal of Applied Physics SPECIAL TOPICS

# Observation of enhanced infrared absorption in silicon supersaturated with gold by pulsed laser melting of nanometer-thick gold films

Philippe K. Chow,[1] Wenjie Yang,[2] Quentin Hudspeth,[1] Shao Qi Lim,[2] Jim S. Williams,[2] and Jeffrey M. Warrender[1,a)]

[1]*US Army Armament Research Development and Engineering Corps-Benet Laboratories, Watervliet, New York 12189, USA*

[2]*Department of Electronic Materials Engineering, Research School of Physics and Engineering, Australian National University, Canberra, Australian Capital Territory 0200, Australia*

(Received 15 November 2017; accepted 18 March 2018; published online 2 April 2018)

We demonstrate that pulsed laser melting (PLM) of thin 1, 5, and 10 nm-thick vapor-deposited gold layers on silicon enhances its room-temperature sub-band gap infrared absorption, as in the case of ion-implanted and PLM-treated silicon. The former approach offers reduced fabrication complexity and avoids implantation-induced lattice damage compared to ion implantation and pulsed laser melting, while exhibiting comparable optical absorptance. We additionally observed strong broadband absorptance enhancement in PLM samples made using 5- and 10-nm-thick gold layers. Raman spectroscopy and Rutherford backscattering analysis indicate that such an enhancement could be explained by absorption by a metastable, disordered and gold-rich surface layer. The sheet resistance and the diode electrical characteristics further elucidate the role of gold-supersaturation in silicon, revealing the promise for future silicon-based infrared device applications.
https://doi.org/10.1063/1.5015984

## I. INTRODUCTION

Silicon doped with impurities (e.g., S, Au) using pulsed-laser melting (PLM) and rapid solidification exhibits sub-bandgap absorption, which could enable more cost-effective and efficient Si-based infrared photodetector and photovoltaic applications. PLM exploits non-equilibrium kinetics in order to trap impurities in the Si lattice at concentrations exceeding the equilibrium solubility limit (i.e., "hyperdoping"), which creates optically-active midgap energy levels. This approach was extensively explored for chalcogen impurities, which were introduced using ion implantation.[1–7] However, negligible sub-band gap device photoresponse was observed, which was attributed to the proximity of the midgap levels to the Si conduction band edge and the broadening of those levels into the band edge at hyperdoping concentrations.[4–6] In response, transition metal impurities were investigated as dopants, due to their deeper midgap levels.[8–12] Initial studies, which focused on the physical nature of transition metal incorporation using ion implantation and PLM, revealed limitations to the approach due to morphological instabilities arising from the transition metals' much greater ability to segregate at the liquid/solid interface as compared with the chalcogens (as quantified by the "diffusive velocity," the ratio of the interface diffusivity to the interface width).[10,13] Above a certain critical impurity concentration in liquid Si, rather than resolidifying as a single-crystal, a characteristic morphology previously observed during constitutional supercooling studies and referred to as "cellular breakdown" is observed, consisting of a crystalline hyperdoped solid separated by "cell walls" that are rich in impurity as compared to crystalline Si.

Gold, having one of the smallest diffusive velocities of the transition metals, was proposed as a plausible candidate impurity due to the ability of PLM to kinetically trap large atomic concentrations ($\sim 10^{18}$–$10^{22}\,cm^{-3}$) in Si through ion implantation and PLM,[9,10] as well as using PLM of vapor-deposited thin (1–10 nm) Au films on Si.[14] The latter approach reduces fabrication complexity and eliminates the necessity to melt beyond the amorphisation or damaged layer as in the case of ion implantation.[10] The technological promise of Au-hyperdoped Si prepared by ion implantation and PLM was demonstrated when an absorption coefficient, $\alpha$, of $\sim 600\,cm^{-1}$ at $\lambda = 1550$ nm (Ref. 9) was first reported for an implantation dose of $10^{15}$ at./cm$^2$. When fabricated into photodiode structures on *n*-type (001) substrates, infrared photoresponse at room temperature was observed. In this work, we demonstrate that Au-hyperdoped Si, prepared using Au thin films deposited on Si, also exhibits sub-band gap absorption comparable to ion-implanted and laser melted Si. We observe strong broadband absorptance enhancement when the initially deposited Au film exceeds a given thickness. Raman spectroscopy and Rutherford backscattering spectrometry (RBS) indicate that such an enhancement could be explained by absorption in a metastable, disordered and Au-rich surface layer. The sheet resistance and the diode electrical characteristics further highlight the potential device applications of Au-supersaturated Si for infrared device applications.

## II. EXPERIMENT

Double-side polished *n*–(phosphorus-doped, 1–5 Ω cm) or *p*-type (boron-doped, 1–10 Ω cm) Si wafers were ultrasonically cleaned in acetone, methanol and isopropanol and dried under ultra-high purity nitrogen. The wafers were subsequently dipped in a buffered-oxide etch (BOE) solution, rinsed in deionized water and dried in nitrogen, and then loaded within one minute of etching (to minimize oxide re-growth) into an electron beam evaporator with a base

[a)]Electronic mail: jwarrend@post.harvard.edu

pressure of $\sim 10^{-5}$ Pa. Nominal thicknesses of 1, 5, and 10 nm were deposited in separate runs, which were monitored using a quartz-crystal microbalance. For comparison, a Si wafer was implanted with Au at 50 keV with an areal dose of $1 \times 10^{15}$ at./cm$^2$, resulting in a peak concentration of $4 \times 10^{20}$ at./cm$^2$ at a depth of 35 nm.

Following thin-film deposition or ion implantation, samples were irradiated with a single pulse from the third harmonic (355 nm) of a Nd:YAG laser (Ekspla) with a pulse duration of 6 ns. A typical sample comprises a region of several individually shot regions adjacent to each other. Prior to harmonic conversion, the fundamental beam was spatially homogenized using relay imaging and an 800 $\mu$m pinhole. The 355 nm beam had a diameter of approximately 8 mm and was used with a 5 mm-square aperture. A variable attenuator was used to adjust the pulse energy density. The laser fluence was calibrated by melting a pristine Si wafer and simultaneously monitoring the melt duration using the time-resolved reflectivity (TRR) of a 488 nm $Ar^+$ ion laser. The melt depth and the fluence (0.8 J/cm$^2$) were then calculated from the measured melt duration using a one-dimensional heat flow simulation. We additionally cut portions from the same sample set and annealed them in flowing argon at 400 °C for 30 min. The initial ramp rate from room temperature was 18.8 °C/min. Samples were cooled to 150 °C at a rate of 25 °C/min, removed from the furnace and placed on a room-temperature steel block.

The thin film transmittance and reflectance were measured in the near infrared region (1000–1800 nm) at room-temperature using a Perkin Elmer UV/vis/NIR spectrophotometer equipped with a 150-mm integrating sphere and an InGaAs detector. Light from a tungsten-halogen lamp was incident on the PLM treated-side of the sample. The average absorptance, $A$, was calculated using three separate measurements of reflectance ($R$) and transmittance ($T$) spectra according to $A = 1\text{-}R\text{-}T$. Raman spectra were measured using a 10-mW, 405-nm, cw laser focused through a 20× microscope objective to a spot size of $\sim$20 $\mu$m on a hyperdoped layer. The backscattered light was directed into a 3000 line/mm diffraction grating and into a photomultiplier tube. The 405-nm excitation line was selected to obtain representative spectra of the whole Au-doped layer, since 514-nm spectra were found to be overly representative of the substrate Si. A 2.0-MeV $^4He^+$ beam was used to perform Rutherford backscattering spectrometry (RBS) on the samples before and after thermal annealing. A glancing detector placed at 78° from the sample surface normal was used to maximize depth resolution. Measurements taken from a direction that is not aligned with any crystallographic axis ("random" spectra) are used to extract the Au distribution profile. Ion channeling measurements taken from the ⟨100⟩ axial channel direction ("channeled" spectra) were used to examine the crystallinity of the Au-hyperdoped layer and the substitutionality of the Au atoms.

Following melting, we fabricated van der Pauw structures in a cloverleaf geometry with a total width of 2.6 mm and a central device diameter of 800 $\mu$m using photolithography and $CHF_3/SF_6$-based reactive-ion etching to a depth of 1.5 $\mu$m to define mesa structures for electrical measurements of Si doped by PLM of a 1-nm-thick Au film. A 250 nm-thick $SiO_2$ field oxide was then deposited by plasma-enhanced chemical vapor deposition (PECVD) at 300 °C for 10 min. Photolithography and 1:10 buffered oxide etch (BOE) were used to pattern and etch square contact windows (180–$\mu$m per side, spaced 1.5 mm apart, see Fig. 4 schematic) in the field oxide. A final photolithography step was used to define 1.8-mm square electrode pads for probing. To ensure intimate contact with the semiconductor, an $O_2$-based plasma removed residual photoresist residue and the sample were dipped in the BOE solution for 5 s to remove residual oxide on the Au-doped Si surface. This treatment also removed $\sim$10 nm of the exposed field oxide. Finally, 300-nm thick titanium electrodes were defined by DC-sputtering and standard liftoff. The sheet resistance and the Hall coefficient were measured using a source current of 2 $\mu$A and a 0.518 T permanent magnet (Accent HL5500PC). The contacts were symmetric and displayed nearly ideal ohmic behavior over a ±1 V polarization range. Through-plane diode measurements were performed using the same titanium top contacts and also employed a eutectic gallium-indium alloy for an ohmic back contact.

## III. DATA AND ANALYSIS

### A. Optical absorption

The solid curves in Fig. 1(a) show the absorptance spectra ($A = 100\%\text{-}T\text{-}R$) of the thin film samples after PLM. The sub-bandgap absorptance is enhanced by Au thin-film deposition and PLM compared to untreated Si. The inset in Fig. 1(a) shows the similarity of the absorptance spectra of the 1-nm Au film sample to the Au-implanted and PLM-treated samples. (Note that for convenience, throughout this paper, we will refer to our samples by the initial thickness of the

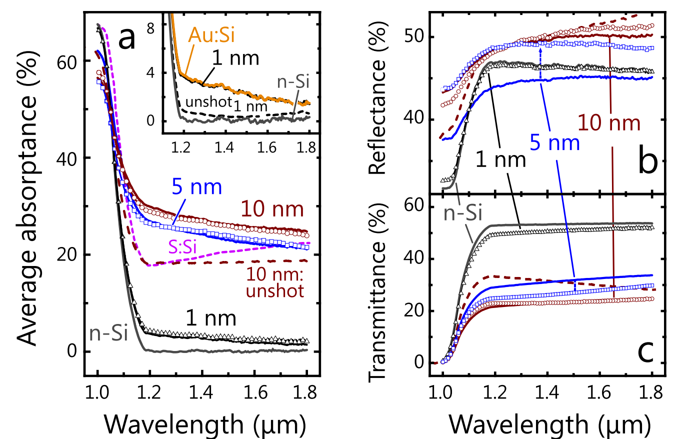


FIG. 1. (a) Absorptance spectra of hyperdoped samples prepared using thin-film deposition and PLM for Au thicknesses of 1 nm (black, solid line), 5 nm (blue, solid line), and 10 nm (maroon, solid line). The spectra of an $n$-type Si wafer (gray, solid line), S-implanted and PLM-treated $p$-Si (Ref. 4) and a 10-nm unshot film (maroon, dashed line) are also shown for reference. Symbols indicate the absorptance spectra measured after annealing in flowing argon at 400 °C for 30 min. The inset shows the similarity of the 1-nm Au thin-film sample to the absorptance of a Au hyperdoped layer prepared by implanting ("Au:Si") 50 keV Au ions at a dose of $10^{15}$ cm$^{-2}$ followed by PLM. Also shown is the unshot 1 nm Au sample (dashed black line). The measured reflectance (b) and transmittance (c) curves show significant deviations of the 5- and 10-nm Au film samples from the reference Si wafer indicating distinctly different surface optical properties from Si.

gold film that was deposited prior to PLM. In the few places where we refer to a film that was deposited but that did *not* receive PLM, we will explicitly refer to them as “unshot.”) This highlights the potential of the thin-film method as an alternative to ion implantation and PLM. The similarity of absorptance profiles for the ion-implanted and thin-film hyperdoped samples suggests that the sub-bandgap absorption in the 1-nm case is due to the substitutional donor-to-conduction band transition previously observed in Au-hyperdoped Si.[9] Our prior secondary ion-mass spectrometry (SIMS) measurements of Au concentration versus depth confirmed that PLM of a thin Au film can achieve comparable supersaturated concentrations in Si,[14] further supporting the argument that Au is responsible for inducing electronic states that enhance the infrared absorption of Si. Near the Si band edge, the Au-doped Si sub-bandgap absorptance increases towards shorter wavelengths as compared to PLM-treated sulfur-implanted *p*-Si[4] [dashed pink curve in Fig. 1(a)], whose absorptance increases towards longer wavelengths, irrespective of the PLM method or implantation dose. This is consistent with the fact that Au induces impurity absorption centers in Si that are energetically deeper in the band gap than with chalcogen impurities, resulting in a larger defect level-to-conduction band transition energy for the former case.[8] We verified that the absorptance enhancement was not solely due to the PLM process by performing the same laser treatment on a pristine *n*-type Si wafer, whose absorptance spectrum was indistinguishable from untreated Si (not shown). The absorptance shows a strong dependence on initially deposited Au film thickness in the 1–10 nm range. For samples for which the initially deposited film was thicker than 1 nm, the absorptance drastically increases across the whole spectral range measured. The absorptance of a PLM-treated 5-nm Au film in this spectral range becomes approximately one order of magnitude higher than that of the 1-nm Au film. An increase in the initial Au film thickness to 10 nm further increases the absorptance. While *R* and *T* spectra of the PLM-treated 1-nm film and the Au-implanted reference sample (not shown) generally resemble those of pristine *n*-type ⟨100⟩ Si (besides the region with absorptance enhancement approaching the Si band edge), the general spectral shapes associated with thicker Au film samples [Figs. 1(b) and 1(c)] contain distinct differences. The sample reflectance differs in magnitude from that of pristine Si, and their profiles change less abruptly near the Si band edge. These observations suggest that the 5- and 10-nm films induce morphological changes to the Si surface that are not observed in the 1-nm case.

Thermal annealing after the PLM step is known to deactivate sub-bandgap absorption in chalcogen-hyperdoped Si.[2,3] For example, after 30 min of annealing at 400 °C in an argon atmosphere, sulfur-doped Si absorptance decreases to approximately half of its magnitude without annealing.[2] Contrary to what was reported for single-crystal chalcogen-hyperdoped Si, the absorptance of Au-film hyperdoped Si remained mostly unchanged with annealing under these conditions [Figs. 1(a)–1(c), open symbols].The thermal treatment increases the reflectance of the 5- and 10-nm films beyond that of Si, while the 1-nm film reflectance does not change within measurement error.

To investigate the origin of the large absorptance enhancement in the thicker Au film samples, we measured the absorptance of 1- and 10-nm Au films which had not undergone PLM treatment. The 10-nm unshot Au film showed a substantial featureless broadband absorptance of ∼18%, while the 1-nm unshot film showed a much smaller broadband contribution of about 1%. This contribution is comparable to the resolution of the instrument. Despite the difference in the magnitude of the broadband contribution, both unshot samples show a lack of absorptance increase towards shorter wavelengths compared to all PLM-treated samples, which do show this increase. This confirms the influence of PLM and gold incorporation on the spectral shape. We suspect an inherently different absorption mechanism dominating in the thicker Au samples. Enhanced infrared absorption in thin metal or metal-silicide films on Si substrates has previously been reported,[15–18] where the authors measured mostly wavelength-independent absorption coefficients on the order of $10^5\,\mathrm{cm}^{-1}$ due to the confinement of electromagnetic radiation. The preservation of the broadband absorptance enhancement with thermal annealing implies that the metallic character of the surface is preserved, suggesting an inhomogeneous morphology in the “thick” film-hyperdoped samples.

### B. Structural characterization

Raman spectroscopy was used to study the morphological characteristics of the samples. The solid curves in Figs. 2(a) and 2(b) show spectra of samples after PLM. We used curve fitting to study the change in the Brillouin-zone-center phonon peak near $520\,\mathrm{cm}^{-1}$ with Au film thickness. The results, shown in Figs. 2(b)–2(d), further highlight the morphological differences in the thicker films. Whereas the peak’s lineshape and intensity are virtually identical to that of pristine Si for the1-nm film, PLM-treated Si, and PLM-treated Au-implanted sample (not shown), the peak intensity is significantly diminished for the 5- and 10-nm films. Additionally, a pronounced

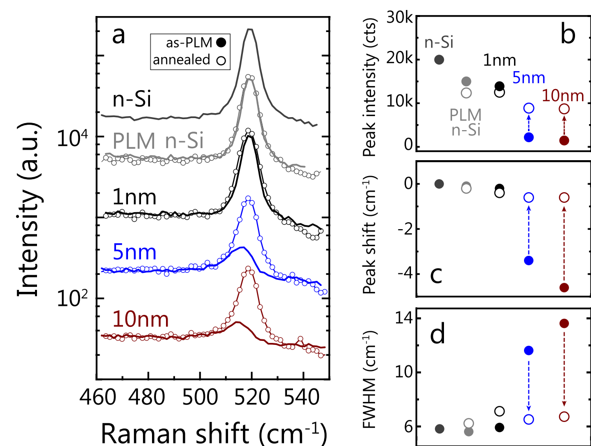


FIG. 2. (a) Raman spectra of thin-film Au hyperdoped Si. Solid curves represent spectra of samples after PLM, while the curves with symbols show spectra of the same samples after thermally annealing at 400 °C for 30 min. (b)–(d) Curve fitting results showing the peak intensity, the frequency shift, and the full-width at half maximum (FWHM), respectively, of the zone-center phonon peak for PLM (filled circles) and annealed (empty circles) samples.

phonon redshift (∼4 cm$^{-1}$), peak broadening, and asymmetry are observed. These observations suggest structural disorder in the films, which has been observed in Si doped with high impurity concentrations of shallow-donor elements[19] and transition metals[20] using pulsed-laser annealing methods. A greater visible light absorption coefficient or surface reflectance could partly explain diminished peak intensity in the thicker-Au samples. We note that no evidence of pressure-induced metastable Si phases, known to arise when using femtosecond laser annealing,[21] was observed in the spectra. Prior SIMS measurements on PLM-treated thin-film samples indicate surface layers of high Au concentration ranging from 20 to 40 at. % in the 5- and 10-nm samples.[14] Further from the surface, the concentration drops off relatively quickly and the profile resembles that of the thinner 1-nm film. At such concentrations, Au incorporation is unlikely to be substitutional in the lattice but could be localized in high concentrations in spatially inhomogeneous regions, as seen in cellular breakdown.[22] This has been observed in Si supersaturated with transition metals using PLM of ion-implanted[10] and metal film-coated Si.[23] Thermal annealing at 400 °C resulted in dramatic changes to the Raman spectra of the thicker Au-film samples. In general, annealing tends to restore the intensity, the peak position, the width (FWHM) and the symmetry of the zone-center phonon peak.

In Fig. 3, we compare the random (dashed curves) and channeled (solid curves) RBS spectra of the PLM-treated 1- and 10-nm films, both before (black curves) and after (red curves) thermal annealing. The large peak near channel number 480 is due to backscattering from Au at the surface. The expanded Au profile in Fig. 3(b) shows a tail from the surface peak indicating incorporated Au. A comparison of the random and channeled Au yields, in this case, indicates high substitutionality of Au in Si after PLM. The substitutional fraction, $S$, was calculated using $(1-\chi_{min}^{Au})/(1-\chi_{min}^{Si})$, where $\chi_{min}$ is the ratio of channeled-to-random yields. An $S$-value of ∼0.74 was calculated just below the surface peak. This sample also exhibits high crystallinity, as its channeled spectrum after PLM is indistinguishable from that of a pristine Si reference sample (blue symbols). In addition, the small peak near channel 270 arises from a thin (native) oxide layer. The 1-nm sample shows negligible change in Au substitutionality or depth distribution after thermal annealing.

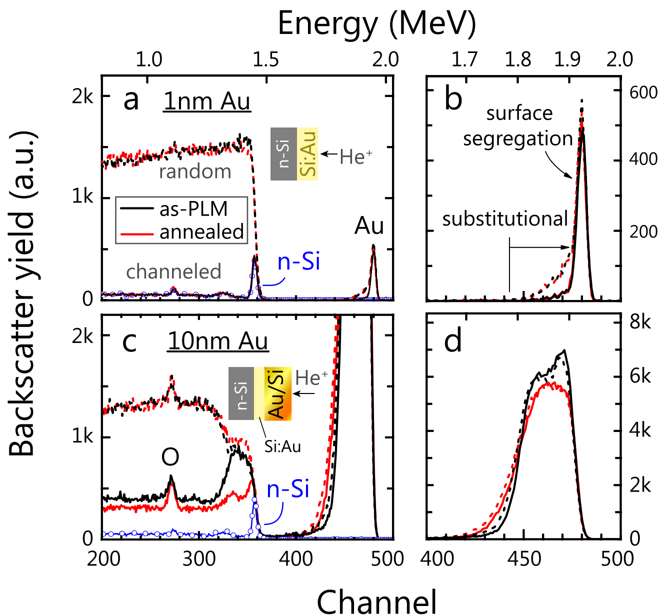


FIG. 3. Rutherford backscattering spectra recorded on hyperdoped Si using 1-nm (a) and 10-nm (c) Au thin films with their respective expanded Au profiles shown in (b) and (d). Samples after-PLM are indicated by black curves, while red curves denote samples annealed at 400 °C for 30 min. The solid curves are the channeled spectra and the dashed curves indicate random spectra. Channeled spectra of a pristine silicon substrate are indicated by the blue curve with open symbols. The spectra indicate a highly substitutional and a crystalline layer (denoted "Si:Au") in the 1-nm case and a thermally sensitive disordered layer (denoted "Au/Si") in the 10-nm case (c).

The 10-nm samples show clear differences from the 1-nm case. The Au profile after PLM in the 10-nm sample spectrum (black curve) has a much higher backscatter yield and is much broader than in the 1-nm samples. The majority of the broad Au profile shows a distinct lack of channeling behavior. The broadening of Au could be a result of either of two causes: some enhanced precipitation (balling up) of Au on the surface after PLM, or the formation of an alloy with Si. The latter seems more likely, as suggested by the lower near-surface Si yield compared with deeper regions of the Si spectra. Indeed, the silicon spectra in the near-surface region show almost no difference between random and channeled cases, indicating the presence of a highly disordered (most likely polycrystalline) Au-Si alloy layer. Simulation of these spectra with the RUMP code indicates that the disordered layer thickness is approximately 70 nm, consistent with prior SIMS measurements of the SiAu layer thickness.[14] This result is also in line with our observation of a redshifted and asymmetric zone-center phonon in the Raman spectra. Upon thermal annealing of the 10-nm sample (red curve), the Au peak slightly decreases in intensity and its backscatter tail extends towards a lower channel number, indicating diffusion away from the surface. The Si near-surface yield in the channeled spectrum is now lower, indicating some grain alignment or improved (single) crystalline quality after thermal annealing.

### C. Electronic characterization

Van der Pauw measurements of the 1-nm thin-film hyperdoped Au samples on n-type substrates generally indicate increased sample sheet resistance upon incorporation of Au using PLM giving an average value of 56 ± 15 kΩ/□. Chalcogen (e.g., S, Se, Te)-hyperdoped layers were shown to exhibit $n$-type conduction and electrical isolation from their $p$-type substrates at room temperature, due to the built-in electric field.[6] We checked for similar rectification, due to hyperdoping with a 1-nm Au film, by measuring the through-wafer current-voltage characteristics [Fig. 4(a)] on the same device, with a simple ohmic back contact formed by mechanically scratching a eutectic gallium-indium ($e$-GaIn) electrode on the rear side of the device. We observed clear rectification in the diode. Therefore, assuming that the hyperdoped film is electronically isolated, due to the rectifying junction formation, a material resistivity of ∼0.3–0.6 Ω cm was calculated by assuming a 50–100 nm thick Si:Au layer (based on prior

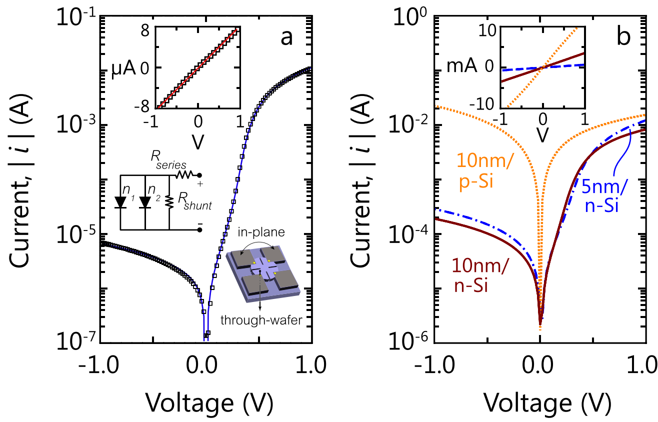


FIG. 4. Electrical characterization of Au thin-film hyperdoped Si. (a) 1-nm Au thin-film van der Pauw structure through-wafer diode current-voltage curve. The top left inset shows the linear in-plane voltage characteristic behavior. The solid blue curve is the resulting parallel circuit model fit (equivalent circuit shown). A to-scale schematic of the cloverleaf mesa geometry used is also shown. (b) Through-waferdiode current-voltage curves of 5- and 10-nm Au film samples (blue, dashed and maroon solid curves, respectively), measured using *e*-GaIn contacts. Also shown in orange (short dashed) is the curve of a PLM-treated 10-nm sample, except on a *p*-type substrate (1–10 Ω cm, boron-doped). No rectification is observed in this sample. The inset shows the corresponding nearly linear in-plane current-voltage curves, indicating low film resistance compared to the 1-nm Au device.

SIMS measurements[14]). This thickness corresponds to the depth where the Au concentration exceeds $10^{18-19}\,\text{cm}^{-3}$. We also verified the presence of an ohmic contact to the hyperdoped layer [inset, Fig. 4(a)], which shows nearly linear in-plane conduction over the same polarization window as the through-wafer measurement. The $\sim$110 kΩ two-probe resistance is comparable to the resistance of a rectangular slab, calculated using the measured sheet resistance, indicating that the contact resistance is small compared to that of the Au:Si material. While some deviation from linearity is observable in this data, it is clearly not responsible for the rectification behavior in the through-wafer measurement. This, combined with our sheet resistance data, suggests the formation of a junction due to the different electronic properties of the hyperdoped layer and the substrate. The measured Hall voltages were overwhelmed by noise, precluding a simple majority carrier type determination, likely due to the large impurity concentration and/or contribution from the substrate carriers. However, our results are consistent with measurements of Au-implanted and PLM-treated Si diodes[9] as well as studies of Au-diffused Si, which showed a conversion to *p*-type conduction and a subsequent decreased resistivity at high Au concentrations.[24] The observed rectification in our devices could arise from a similar p-type conversion or alteration of the Si bandgap due to Au incorporation. The forward bias diode characteristics contain three distinct regimes corresponding to carrier recombination in the space charge region and in the quasi-neutral region, as well as a series resistance-limited current at a high forward bias. We employed a parallel-circuit model including two parallel Shockley diodes[25] in parallel with a shunt resistance ($R_{\text{shunt}}$) and in series with a series resistance component ($R_{\text{series}}$). The calculated diode ideality factors were $n_1 = 0.98$ and $n_2 = 2.80$, characteristic of recombination in the bulk, or the quasi-neutral region, and defect-mediated carrier recombination in the space-charge region, consistent with Au-induced midgap levels or bands, respectively. Fitting also gave values of $R_{\text{shunt}}$ and $R_{\text{series}}$ of $1.6 \times 10^5$ and 50 Ω, respectively. The reverse saturation currents were 1.2 $\mu$A/cm$^2$ for the ideal diode ($n_1$) and 2.5 mA/cm$^2$ for the non-ideal diode ($n_2$). Despite successful junction formation, the anomalously high ($n > 2$) ideality factor could be a result of the finite contact resistance between titanium and the 1-nm Au-doped Si layer,[26] a characteristic feature of carrier recombination in heavily gold-supersaturated Si or the result of a non-abrupt p-n junction due to the tail of the gold concentration profile.[14]

We employed a simpler contacting procedure for studying the 5- and 10-nm film samples' electrical behavior. Although exposure to elevated processing temperatures not exceeding 300 °C was assumed to not significantly alter the properties of the 1 nm Au film-doped samples, based on our absorptance, Raman and RBS data, we could not safely assume this for the 5- and 10-nm Au film samples due to their relative thermal instability. Instead, these samples were cut into 5-mm square chips and probed, without any further processing after PLM, by simply contacting with *e*-GaIn electrodes (without mechanical abrasion). The linear in-plane current-voltage curves [inset, Fig. 4(b)] indicated significantly reduced sample resistance compared to the 1-nm case. Van der Pauw measurements gave sheet resistances of $\sim$1.1 and 0.5 kΩ/□ for the 5- and 10-nm films, respectively, contrasting 1-nm Au samples described above. This direct-probe measurement method was not possible for the 1-nm film due to $\sim$MΩ-scale sample resistances, which gave anomalous voltage readings. The through-wafer diode characteristics were also measured using an ohmic *e*-GaIn back contact. Both the 5- and 10-nm film samples exhibited rectification but did not rectify current as strongly as the 1-nm case. Fitting the data to an ideal diode model was not successful, further suggesting that a metal-semiconductor contact is not responsible for the rectification. Our RBS and prior SIMS measurements support the existence of a comparably Au-hyperdoped layer beneath the disordered Au-Si near-surface layer which, according to our electrical characterization of the 1-nm films, has a *p*-type character. In comparing the in-plane and through-wafer measurements, it is reasonable to conclude that the disordered, intermixed surface layer acts as a semi-metallic contact to the relatively *p*-type hyperdoped layer beneath it, exhibiting rectifying behavior through the underlying n-Si. We measured the current-voltage characteristics of a 10-nm Au film deposited onto *p*-type Si in the same evaporation run as the n-type samples and PLM-treated with the same fluence on the same day. As expected, no rectification was observed in this case.

## IV. DISCUSSION

Our results show an enhancement in sub-bandgap optical absorptance due to the incorporation of Au impurities from thin vapor-deposited Au films into the Si lattice using PLM. A striking broadband absorptance enhancement is observed in 5- and 10-nm Au films, and our material characterization points to distinct morphological characteristics of

these thicker Au film samples, which in turn indicates two different absorption mechanisms. One mechanism involves substitutional hyperdoping of Au in Si, which takes place in gold-implanted and PLM-treated Si. We believe that since our thinnest gold film studied (1-nm) exhibits comparable substitutional supersaturated gold concentrations and exhibits an almost-identical absorptance profile, the same mechanism is responsible. However, when the thickness of the deposited gold film increases, a second mechanism begins to participate. As previously described, this broadband absorption mechanism is due to electronic confinement in very thin metal films on Si. Although the disordered surface of our thicker films (5- and 10-nm) is not pure Au, they remain sufficiently thin (tens of nanometers) and highly conductive with high gold content, satisfying the requirements for the onset of broadband absorption.

RBS and Raman analysis revealed that a disordered Au-Si layer forms after PLM of thick Au films compared to the thinner 1 nm film, which exhibited excellent resolidification and impurity substitutionality. The disordered layer formation is likely a direct result of the PLM and the resolidification process using the thin-film application of impurity. A significantly larger Au impurity concentration in the melt presumably leads to a breakdown of liquid phase epitaxy and polycrystallinity of the alloy during resolidification as we discuss below, and hence this behavior gives rise to the observed structural differences. Conventional explanations of impurity in Si solidification assume a bulk liquid far from the liquid/solid interface that is dilute in impurity. When this bulk liquid exceeds a critical concentration, the interface becomes unstable. Melting with a thin film of a metal with a melting temperature lower than that of Si fundamentally differs from melting an ion-implanted layer, because the solidification begins with a molten layer of pure impurity sitting on the Si surface. If interdiffusion is rapid, the impurity from the molten film will quickly intermix with the Si melt beneath it; however, a thick layer may act as a source of impurity throughout the (silicon) solidification, and the bulk liquid concentration may therefore be well above the dilute solution approximation. Moreover, this high impurity concentration could reduce the undercooling in the liquid, reducing the driving force for solidification. This interpretive picture is supported by the three- to five-fold longer melt durations for the 5- and 10-nm films measured by time-resolved reflectivity (TRR) compared to the 1-nm and pristine Si samples.

To imagine how the top Au-rich molten layer resolidifies to accommodate such large impurity concentrations, the conventional impurity-host liquid-phase epitaxy picture must be abandoned. At some depth, quasi-epitaxial regrowth halts. RBS analysis indeed indicates a disordered intermixed Au/Si layer in the 10-nm film sample, but the asymmetry in the zone-center Raman peak suggests the presence of strained and almost certainly micro-/nano-crystalline Si as well. In accordance with this picture, RBS analysis also indicates some substitutional Au beneath the disordered layer in the 10-nm film sample, indicating some degree of traditional kinetic impurity trapping in the initial stages of solidification. Upon thermal annealing slightly above the Si-Au eutectic temperature, improved crystallization is indicated by both RBS and Raman measurements, which is supported by prior literature concerning metal-induced low-temperature crystallization of disordered amorphous Si films.[27] The persistence of broadband absorptance enhancement of thick samples through thermal annealing indicates that the enhancement is likely not solely due to the disordered Si, but to residual low-dimensional Au[28] or thin Au-rich Si intermixed or alloy layers.

## V. SUMMARY

We have demonstrated that Au thin-film deposition and PLM can be used to enhance sub-bandgap absorptance in silicon, and that the film thickness affects the origin of absorption. We employed Raman spectroscopy, RBS and electrical measurements to demonstrate structural differences between samples formed using PLM of thin and thick Au films. Thermal annealing results further highlighted the morphological differences between the crystalline and disordered layers. We showed that this doping method can be used to form highly crystalline rectifying junctions in *n*-type Si with enhanced sub-bandgap near-infrared absorption. With this approach, the absorbing layer thickness could be further enhanced by increasing the thickness of the Au film, by using, for example, several cycles of depositing Si, depositing Au, and PLM. These results hold promise for the utility of thin-film hyperdoped Si for infrared photodetection and intermediate band photovoltaics. It will be necessary to determine whether the broadband absorptance enhancement in the surface layer can contribute to device photocurrent and how the thermal instability of the surface layer morphology affects device contacting schemes. Spectrally resolved diode responsivity and quantum efficiency measurements, coupled with temperature-dependent electrical characterization, will help to more fully correlate processing parameters to electronic behavior in order to evaluate the potential of thin-film-doped Si for infrared device applications.

## SUPPLEMENTARY MATERIAL

See supplementary material, Fig. 1, for a schematic process flow for 1-nm Au/n-Si devices.

## ACKNOWLEDGMENTS

The authors are thankful to Professor Ishwara Bhat and Dibyajyoti Mohanty for helping with electrical characterization and for useful discussions, as well as Dr. Deniz Rende for providing spectral characterization facility access.

[1]T. G. Kim, J. M. Warrender, and M. J. Aziz, Appl. Phys. Lett. **88**, 241902 (2006).
[2]C. B. Simmons, A. J. Akey, J. J. Krich, J. T. Sullivan, D. Recht, M. J. Aziz, and T. Buonassisi, J. Appl. Phys. **114**, 243514 (2013).
[3]I. Umezu, J. M. Warrender, S. Charnvanichborikarn, A. Kohno, J. S. Williams, M. Tabbal, D. G. Papazoglou, X.-C. Zhang, and M. J. Aziz, J. Appl. Phys. **113**, 213501 (2013).
[4]C. B. Simmons, A. J. Akey, J. P. Mailoa, D. Recht, M. J. Aziz, and T. Buonassisi, Adv. Funct. Mater. **24**, 2852 (2014).
[5]E. Ertekin, M. T. Winkler, D. Recht, A. J. Said, M. J. Aziz, T. Buonassisi, and J. C. Grossman, Phys. Rev. Lett. **108**, 026401 (2012).

[6]M. T. Winkler, D. Recht, M.-J. Sher, A. J. Said, E. Mazur, and M. J. Aziz, Phys. Rev. Lett. **106**, 178701 (2011).
[7]J. M. Warrender, Appl. Phys. Rev. **3**, 31104 (2016).
[8]S. M. Sze, *Physics of Semiconductor Devices*, 3rd ed. (Wiley-Interscience, Hoboken, NJ, 2007).
[9]J. P. Mailoa, A. J. Akey, C. B. Simmons, D. Hutchinson, J. Mathews, J. T. Sullivan, D. Recht, M. T. Winkler, J. S. Williams, J. M. Warrender, P. D. Persans, M. J. Aziz, and T. Buonassisi, Nat. Commun. **5**, 3011 (2014).
[10]D. Recht, M. J. Smith, S. Charnvanichborikarn, J. T. Sullivan, M. T. Winkler, J. Mathews, J. M. Warrender, T. Buonassisi, J. S. Williams, S. Gradečak, and M. J. Aziz, J. Appl. Phys. **114**, 124903 (2013).
[11]J. Olea, M. Toledano-Luque, D. Pastor, G. González-Díaz, and I. Mártil, J. Appl. Phys. **104**, 16105 (2008).
[12]J. Olea, A. del Prado, D. Pastor, I. Mártil, and G. González-Díaz, J. Appl. Phys. **109**, 113541 (2011).
[13]J. M. Warrender, J. Mathews, D. Recht, M. Smith, S. Gradečak, and M. J. Aziz, J. Appl. Phys. **115**, 163516 (2014).
[14]J. M. Warrender, Q. Hudspeth, G. Malladi, H. Efstathiadis, and J. Mathews, Appl. Phys. Lett. **109**, 231104 (2016).
[15]G. D. Mahan and D. T. F. Marple, Appl. Phys. Lett. **42**, 219 (1983).
[16]W. Lang, K. Kühl, and H. Sandmaier, Sens. Actuators, A **34**, 243 (1992).
[17]T. Turbadar, Proc. Phys. Soc. **73**, 40 (1959).
[18]J. M. Mooney, J. Appl. Phys. **64**, 4664 (1988).
[19]K. P. Jain, A. K. Shukla, R. Ashokan, S. C. Abbi, and M. Balkanski, Phys. Rev. B **32**, 6688 (1985).
[20]D. Pastor, J. Olea, A. del Prado, E. García-Hemme, I. Mártil, G. González-Díaz, J. Ibáñez, R. Cuscó, and L. Artús, Semicond. Sci. Technol. **26**, 115003 (2011).
[21]M. J. Smith, Y.-T. Lin, M.-J. Sher, M. T. Winkler, E. Mazur, and S. Gradečak, J. Appl. Phys. **110**, 53524 (2011).
[22]A. J. Akey, D. Recht, J. S. Williams, M. J. Aziz, and T. Buonassisi, Adv. Funct. Mater. **25**, 4642 (2015).
[23]G. J. van Gurp, G. E. J. Eggermont, Y. Tamminga, W. T. Stacy, and J. R. M. Gijsbers, Appl. Phys. Lett. **35**, 273 (1979).
[24]H. Weman, A. Henry, T. Begum, B. Monemar, O. O. Awadelkarim, and J. L. Lindström, J. Appl. Phys. **65**, 137 (1989).
[25]C. Sah, R. Noyce, and W. Shockley, Proc. IRE **45**, 1228 (1957).
[26]J. M. Shah, Y.-L. Li, T. Gessmann, and E. F. Schubert, J. Appl. Phys. **94**, 2627 (2003).
[27]L. Hultman, A. Robertsson, H. T. G. Hentzell, I. Engström, and P. A. Psaras, J. Appl. Phys. **62**, 3647 (1987).
[28]N. Ferralis, R. Maboudian, and C. Carraro, J. Am. Chem. Soc. **130**, 2681 (2008).